Model Predictive Direct Torque Control With Finite Control Set for PMSM Drive Systems, Part 2: Field Weakening Operation

Matthias Preindl and Silverio Bolognani, *Member, IEEE*

***Abstract*—The direct torque control approach called *model predictive direct torque control* (MP-DTC) is extended to field-weakening operation in this research. The controller is of the finite control set (FCS) type, which takes the discrete states of the voltage source inverter (VSI) into account. Each sampling period, the future behavior of the plant is predicted and inputs (voltage vectors) are selected using an optimization criterion, i.e., a cost function. Optimization, however, depend on the operation region. Maximum torque per ampere (MTPA) tracking for high electrical efficiency is aimed below rated speed, operation off the MTPA trajectory is necessary for obtaining field-weakening. In this work, a cost function is designed, which is suitable for operation at high speeds without penalizing operation below rated speed. MP-DTC is applied to permanent magnet synchronous machine (PMSM) drive systems. High control performances, i.e., dynamics, is obtained without increasing the switching frequency nor reducing significantly the torque quality. This feature is interesting above all for high power applications. The proposed control strategy has been evaluated on a small-scale (PMSM) drive system with two-level VSI for demonstration showing promising results.**

***Index Terms*—Drive systems, field-weakening, internal permanent magnet synchronous machine (IPM), model predictive control (MPC).**

NOMENCLATURE

$R \in \mathbb{R}_+$	Stator resistance $[\Omega]$
$L_d, L_q \in \mathbb{R}_+$	Stator inductance (d, q axis, resp.) $[H]$
$\psi \in \mathbb{R}_+$	PM flux linkage $[Wb]$
$B \in \mathbb{R}_+$	Friction coefficient $[kgm/s^2]$
$J \in \mathbb{R}_+$	Inertia coefficient $[kgm^2]$
$u_d, u_q \in \mathbb{R}$	Stator voltage (d, q axis, resp.) $[V]$
$i_d, i_q \in \mathbb{R}$	Stator current (d, q axis, resp.) $[A]$
$U_r \in \mathbb{R}_+$	Rated stator voltage $[V]$
$I_r \in \mathbb{R}_+$	Rated stator current $[A]$
$U_c \in \mathbb{R}_+$	DC-link voltage $[V]$
$N_u \in \mathbb{N}_+$	Number of inverter switching states
$\theta \in \mathbb{R}$	Electrical rotor angle $[rad]$
$\omega \in \mathbb{R}$	Electrical rotor speed $[rad/s]$
$n \in \mathbb{R}$	Electrical rotor speed $[rpm]$
$T_e \in \mathbb{R}$	Electrical torque $[Nm]$
$T_l \in \mathbb{R}$	Load torque $[Nm]$
$t \in \mathbb{R}_+$	Time $[s]$
$T_s \in \mathbb{R}_+$	Sampling period $[s]$
$k \in \mathbb{N}_+$	Sample
$N \in \mathbb{N}_+$	Prediction horizon
$T_x \in \mathbb{R}_+$	Execution time $[s]$
$f_{sw} \in \mathbb{R}_+$	Switching frequency $[Hz]$
$f_{swp} \in \mathbb{R}_+$	Theoretic peak switching frequency $[Hz]$
$.^*$	Reference value
$x \in \mathbb{R}^n$, $n \in \mathbb{N}_+$	Plant states
$u \in \mathbb{R}^m$, $m \in \mathbb{N}_+$	Controlled plant inputs
$y \in \mathbb{R}^r$, $r \in \mathbb{N}_+$	Measurements
$\mathbf{A} \in \mathbb{R}^{n \times n}$	State parameter matrix
$\mathbf{B} \in \mathbb{R}^{n \times m}$	Input parameter matrix
$\mathbf{E} \in \mathbb{R}^{n \times p}$	Disturbance parameter matrix
$\mathbf{C} \in \mathbb{R}^{r \times n}$	Measurement parameter matrix

Manuscript received December 09, 2011; revised February 02, 2012, March 10, 2012, and June 11, 2012; accepted June 14, 2012. Date of publication September 24, 2012; date of current version January 09, 2013. Paper no. TII-11-0996.R3.

The authors are with Department of Industrial Engineering, University of Padova, 35131 Padova, Italy (e-mail: matthias.preindl@gmail.com; bolognani@die.unipd.it).

Color versions of one or more of the figures in this paper are available online at http://ieeexplore.ieee.org.

Digital Object Identifier 10.1109/TII.2012.2220353

I. INTRODUCTION

MODEL predictive control (MPC) is a control concept which uses a system model to predict the future system states in discrete time steps. A constant and finite number of future states are predicted, where the number is called *prediction horizon* N [1]. MPC is also called receding horizon control since N is constant with respect to the actual sampling instant,

i.e., it moves over the time. After prediction, the optimal control action should be selected. Of course, optimality can be obtained only with respect to a mathematical formulation, which is the cost function [2]. This function is designed with respect to the problem statement and it is used to choose the plant input. Moreover, MPC can handle complex problem statements including nonlinear systems, MIMO systems, and system constraints in an unified manner. This capability makes it fairly special and it is appreciated by many scientists [3].

Different MPC strategies have been proposed in literature. Prediction and computation of the cost function can be very time-consuming. Thus, the problem can be solved online or offline leading to strategies, which are called realtime [4]–[6] or explicit MPC [3], [7], respectively. Sampling time scales in power electronic and drive applications are usually fairly small. Thus, the prediction horizon of on-line MPC implementations must be limited to a few periods [2].

Moreover, a power electronic converter has a discrete set of switching states, i.e., plant inputs. Thus, MPC can be of the continuous control set (CCS) type, which means the converter is linearized using a modulation scheme [8], e.g., pulse width modulation PWM [9]. Concepts which take into account the discrete nature of the device are called Finite Control Set (FCS) MPC [10], [11].

Many applications of MPC in the area of power electronics and drives are shown in literature [12] including low-power, servo drives [7], [13], [14], rectifiers [15], [16], high power converters [17], [18]. In high power systems, the semiconductor devices have high switching losses and require low switching frequencies. Modulation schemes couple switching and sampling frequency limiting the possible dynamics of the system above all if linear controllers are used. Strategies, which apply directly voltage vectors are, e.g., hysteresis based [19], [20] controllers. A typical drawback of this strategies is the reduction of the current and torque quality.

MP-DTC concept is proposed as an alternative to these control schemes aiming high dynamic performance without reducing the current and torque quality. The concept takes the discrete nature of the converter into account and it is therefore from the FCS-MPC type. The concept aims high power applications in first place. Examples are traction (train, tram) [21], ship propulsion [22], and renewable energy power plants (wind power) [23]. Anyway, the concept is not limited to high power applications, but the lower switching frequencies allow lower sampling times. Thus, demands on execution time are relaxed.

Over-speed capabilities are required in several applications like traction, power generation, etc. Therefore, MP-DTC must be suitable for field-weakening. Traditional field-weakening concepts [24], [25] are separated from the current and speed control. They introduce an additional negative d-current which produces a voltage drop which opposes the rotor flux resulting in a lower stator voltage. However, such an explicit formulation cannot be combined with MP-DTC since the d-current cannot be directly set because it is an internal control variable. An implicit formulation is required and is introduced into the cost function. Moreover, control goals depend on the type of operation of the machine. Below rated speed, a PMSM should work on the maximum torque per ampere (MTPA) trajectory

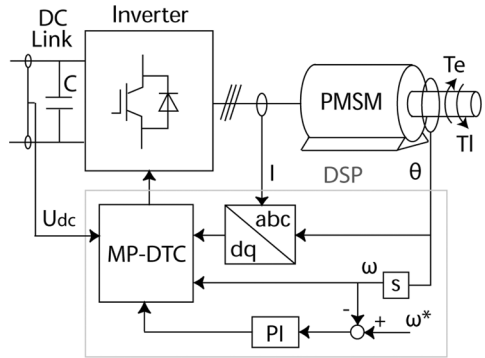

Fig. 1. PMSM-VSI drive sytem.

for obtaining high electrical efficiency. Above rated speed, operation off the MTPA trajectory is required for obtaining higher speeds. The preferable operation conditions in this regions are defined and implemented.

This paper is organized as follows. The plant is analyzed in Section II and the main control goals are defined in the same section. In Section III, an overview of the MP-DTC controller design is given and the design for field weakening is shown. The simulation and experimental results are shown in Section IV. The paper is concludes with a summary in Section V.

II. Analysis

A. Plant

The stator equations of a generic permanent magnet synchronous machine (PMSM) model is in the rotating (dq) reference frame and continuous time

$$\begin{aligned} \dot{i_d} &= -\frac{R}{L_d} i_d + \frac{L_q}{L_d}\omega i_q + \frac{1}{L_d} u_d \\ \dot{i_q} &= -\frac{R}{L_q} i_q - \frac{L_d}{L_q}\omega i_d + \frac{1}{L_q} u_q - \frac{\psi}{L_q}\omega. \end{aligned} \tag{1}$$

The torque equation is

$$T_e = \frac{3}{2} p(\psi i_q + (L_d - L_q) i_d i_q) \tag{2}$$

and the mechanical equations are

$$\begin{aligned} \dot{\omega} &= -\frac{B}{J}\omega + \frac{p}{J}(T_e - T_l) \\ \dot{\theta} &= \omega. \end{aligned} \tag{3}$$

For controlling the currents, (1) is from interest, which can be written in the state-space form

$$\begin{aligned} \dot{x}(t) &= \mathbf{A}x(t) + \mathbf{B}u(t) + \mathbf{E} \\ y(t) &= \mathbf{C}x(t) \end{aligned} \tag{4}$$

where $x = [i_d, i_q]^T$, $u = [u_d, u_q]^T$, and

$$\mathbf{A} = \begin{bmatrix} -\frac{R}{L_d} & \omega\frac{L_q}{L_d} \\ -\omega\frac{L_d}{L_q} & -\frac{R}{L_q} \end{bmatrix} \quad \mathbf{B} = \begin{bmatrix} \frac{1}{L_d} & 0 \\ 0 & \frac{1}{L_q} \end{bmatrix}$$

$$\mathbf{E} = \begin{bmatrix} 0 \\ -\omega\frac{\psi}{L_q} \end{bmatrix} \quad \mathbf{C} = \begin{bmatrix} 1 & 0 \\ 0 & 1 \end{bmatrix}$$

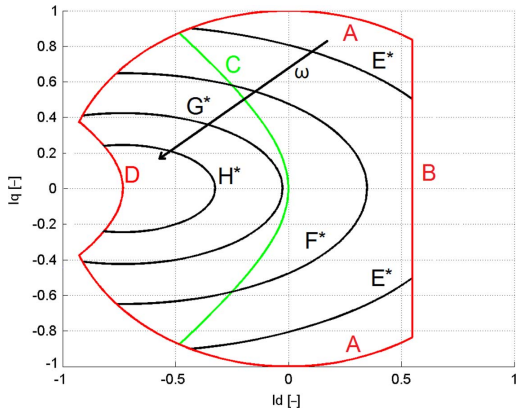

Fig. 2. MP-DTC state plane in pu values: A—current limit; B—MTPA condition stability limit; C—MTPA trajectory; D—MTPV trajectory; E*—constant torque operation; F*—constant power operation 1: voltage limit cuts the MTPA trajectory; G*—constant power operation 2: voltage limit cuts neither MTPA nor MTPV trajectory, flux weakening is necessary in no-load conditions; H*—reduced power operation: maximum torque is not produced by rated current but on MTPV trajectory; (*) marked trajectories are speed dependent and vary with the arrow ω.

ω is a parameter in this model, which holds if the mechanical and electrical time constant differs significantly, which is the case in most practical applications. Since torque control is focused, (2) is also used for control.

A voltage source inverter (VSI) is used for power conversion, which sets the stator voltage, i.e., the plant inputs. Since no modulation scheme is used, it can apply a finite set of voltages U to the motor, i.e., $u(t) \in U \subset \mathbb{R}^m$. Moreover, the application period of voltage vectors is known, i.e., the possible electrical states are $x(t) \in X \subset \mathbb{R}^n$. In other words, the possible inputs are a finite set leading to a finite set of future states, which can be computed with respect to the inputs and measurements.

B. Control

MP-DTC is a controller aiming practical asymptotic stability [26] and practical torque reference tracking $\lim_{t\to+\infty} \|x - x^*\| < \epsilon$. These goals are obtained considering the plant limits of states and inputs. Moreover, additional control goals are taken into account such as MTPA tracking.

C. Field Weakening

Below rated speed, MP-DTC works on the MTPA trajectory. In this case, the inverter voltage is always sufficient to control the stator currents. Rated torque can be obtained independently from the machine speed. Below rated speed, the amplitude of the currents need to be limited (trajectory A in Fig. 2). Moreover, the solution of the MTPA [see (7)] is not unique, i.e., it is symmetric with respect to $i_d = 2(L_d - L_q)/(\psi)$. In order to force the states to convergence to the correct solution, operation is limited to $i_d < 2(L_d - L_q)/(\psi)$ (trajectory B in Fig. 2). Operation below rated speed is shown in detail in [27].

In various applications, the rated speed must be exceeded accepting a reduction of the maximal available torque. In this case the steady-state terminal voltage exceeds the maximum admissible one, which is given by the DC-link voltage. In order to reduce the terminal voltage, a negative d-axis current is introduced. This current leads to a voltage drop, which counterbalances the electromotive force (emf) generated by the rotor flux. With this principle arises the so called field weakening operation.

Traditional field weakening concepts use the d-axis currents as plant input [24]. For flux weakening, i.e., decreasing the stator voltage, a negative i_d current is injected. This concept works if $id > -(\psi)/(Ld)$. Beyond this limit, i.e., $id < -(\psi)/(Ld)$, also a reduction of the q-axis current is required for decreasing the stator voltage. Thus, $id > -(\psi)/(Ld)$ defines the stable operation region for such concepts. More advanced concepts may act on the current angle or both currents assuming that an increase of the absolute current corresponds to an increase of torque [24]. In this case, the stable region is slightly extended but the MTPV curve (trajectory D in Fig. 2) becomes the stability limit. This limit is given by the fact that on the left side of the MTPV trajectory, an increase of the absolute current does not correspond to an increase of the torque but to a decrease. Thus, a state-of-the-art field weakening controller should be stable at the right-hand side of the MTPV criteria (trajectory D in Fig. 2) for exploiting the physically possible range but avoid operation at the left-hand side since it leads to lower torques with higher currents.

MP-DTC is not suitable for such approaches since the d-current cannot be explicitly set and no average voltage is available for measurement. For this reason, an implicit handling of the field-weakening concept is implemented. Using the implicit formulation, stability (at the right-hand side of the MTPV criteria) is given. Operation at the left-hand side of the MTPV criteria is avoided introducing it as constraint (trajectory D in Fig. 2).

Field weakening is obtained introducing the voltage limit into the electrical, i.e., MP-DTC state plane

$$|\omega|\sqrt{(L_q i_q)^2 + (L_d i_d + \psi)^2} < U_r \tag{5}$$

which is obtained assuming steady state conditions $\dot{x}(t) \equiv 0$ and zero resistances. These assumptions lead to a d-axis symmetric criteria. Thus, the electrical states are limited by the trajectories A, B, and D in Fig. 2, which are constant and independent from the operating conditions of the electrical machine. On the other hand, the speed limit varies and it has a different influence on the electrical machine, which depends on the speed. Examples for the speed limit are the trajectories E^*, F^*, G^*, and H^* in Fig. 2 for different speeds, where $(*)$ indicates that the limit changes with ω. Of course, during operation only one trajectory is active and its location must be calculated given the speed ω.

With respect to voltage limit, i.e., the PMSM speed, four operating conditions can be identified:

- *Constant torque operation*: MP-DTC works on the MTPA trajectory (trajectory C in Fig. 2) below rated speed for high efficiency. The voltage limit (trajectory E in Fig. 2) does not influence the operation. Constant torque operation happens if the voltage limit (e.g., trajectory E^* in Fig. 2) stays on the right of the MTPA trajectory (trajectory C in Fig. 2). In this case, the electrical states x are forced to be in the area delimited by the trajectories A, B, D, and E^*.
- *Constant power (volt-ampere) operation 1*: The maximum torque must be reduced, since the terminal voltage must be limited to its rated value beyond rated speed. How-

ever, rated apparent power can be obtained. This region is characterized by the voltage limit which cuts the MTPA trajectory. For obtaining high efficiency, the states should lay on the MTPA trajectory in the case of operation with low torques. In the case of high torques, they should stay close to the voltage limit. In contrast to the other regions, two potentially conflicting operating conditions (close to MTPA and voltage trajectory, which are trajectory C and F in Fig. 2, respectively) are aimed in this region. The preferable one depend on the required electrical torque. Thus, constant power (volt-ampere) operation 1 happens if the voltage limit (e.g., trajectory F^* in Fig. 2) intersects the MTPA trajectory (trajectory C in Fig. 2). In this case, the electrical states x are forced to be in the area delimited by the trajectories A, D, and F^*.

- *Constant power (volt-ampere) operation 2*: Also in this case, the peak torque must be reduced according to the voltage limit. This region is characterized by a voltage limit, which cuts neither the MTPA (trajectory C in Fig. 2) nor the MTPV (trajectory D in Fig. 2) trajectory. The voltage limit, i.e., flux weakening is always active even in no load conditions. Thus, constant power (volt-ampere) operation 2 happens if the voltage limit (e.g., trajectory G^* in Fig. 2) stays on the left of the the MTPA trajectory (trajectory C in Fig. 2) and the voltage limit ends cutting the peak current limit (trajectory A in Fig. 2). In this case, the electrical states x are forced to be in the area delimited by the trajectories A, D, and G^*.
  A distinction between constant power operation 1 and 2 becomes necessary since the goals for obtaining high efficiency at low torques (low absolute currents) changes. In the first case, operation close to the MTPA trajectory should be aimed. In the latter case, this operation is not possible anymore and the operation close to the voltage limit is aimed.
- *Reduced power (volt-ampere) operation*: At even higher speed, there exists a conceptual limit where the torque cannot be increased anymore. This limit is given by the MTPV trajectory (21) and it is shown as trajectory D in Fig. 2. On the left side of the trajectory, the torque decreases and operation becomes disadvantageous. Accordingly the peak current is limited to the left side of the MTPV trajectory. Thus, reduced power (volt-ampere) operation happens if the voltage limit (e.g., trajectory H^* in Fig. 2) stays on the left of the MTPA trajectory (trajectory C in Fig. 2) and the voltage limit ends cutting the MTPV limit (trajectory D in Fig. 2). In this case, the electrical states x are forced to be in the area delimited by the trajectories D, and H^*.

The cases are shown in Fig. 2.

III. Synthesis

The extension of MP-DTC to field-weakening operation is shown in this section. First, a brief outline of the basic controller is shown. Then, the required modifications of the controller are shown.

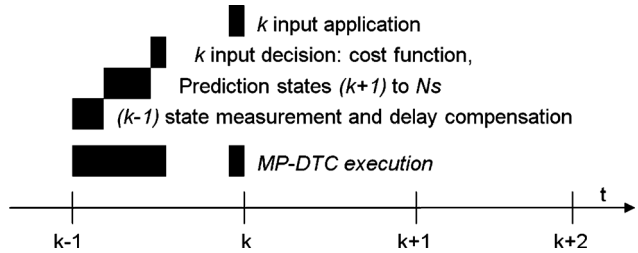

Fig. 3. Execution of the MP-DTC algorithm.

A. MP-DTC Outline

The controller works in four basic steps. The controller is executed in sampling instant $k-1$, based on the measurements in sampling instant $k-1$ and the controller sets the plant input in sampling instant k. After measurement $(k-1)$, the execution delay ($k-1$ to k) is compensated [28]. The second step is the prediction of the plant states up to prediction horizon $(k+1),\ldots,N$ and the third step is the selection of the plant input for sampling instant k. Finally, the controller actuates the plant input at sampling instant k. The MP-DTC execution is shown in Fig. 3.

1) Measurement: The measurement $y(k-1)$ is manipulated due to the plant input $u(k-1)$ and the plant itself $x(k-1)$. Since the execution time T_x of the controller is finite, a unit delay is introduced by the controller between the measurement in $k-1$ and the actuation in k. Since the states may be manipulated significantly during the delay, compensation of the measurement from $k-1$ to k is necessary. Thus, the actual states $\hat{x}(k)$ are calculated using the measurement $y(k-1)$ and the inputs $u(k-1)$.

Moreover, noise and not modeled sensor delay can influence significantly the steady-state performance resulting in large ripples. For this reason, e.g., Kalman filters [29] can be used. In this research, a Luenberger observer [30] is preferred due to its simplicity. Introducing an integrative part to the observer, steady-state prediction offsets are avoided, too. The observer is described in detail in [27].

2) Prediction: The possible inputs of a power converter without modulator are a finite set $U(k)$ of u_d and u_q combinations leading to a finite set of future states $X(k+1)$, which can be computed. Using a recursive function, the possible future states can be calculated up to the prediction horizon N. However, the number of predictions increases exponentially with the prediction horizon $(N_u)^N$. Thus, the prediction horizon must be limited to a few sampling periods for a real time implementation.

The number of predictions can be limited using a state graph [5]. The future states are limited to the converter switch states, which can be reached with the modification of a single leg state change. In other words, if a given vector is applied in a sampling period, the vector itself, the neighbor vectors, and a zero vector is available in the next period. The switching graph has additional benefits. The average switching frequency is limited since only one switch change is permitted per sampling period. The theoretic peak switching frequency is [5] $f_{swp}=(6T_s)^{-1}$. Moreover, the application of two opposite voltage vectors, the so called bipolar switching, is avoided.

3) Selection: The future plant input is selected using a cost function. The function must choose the optimal one between the ones, which has been predicted. Of course, optimality can be obtained only with respect to a criteria, i.e., a mathematical function.

The cost function is subdivided in three criteria. First, a tracking criteria is designed. Since the controller aims the tracking of the torque reference, the goal is the minimization of the relative error

$$c_T(k) = (T_e(k) - T_e^*(k))^2 \tag{6}$$

which is the main component of the cost function.

Torque can be obtained by various combinations of the electrical states x. However, there are preferences how the torque should be generated. Thus, the second criteria introduces an attraction region in the state plane. Low current is, e.g., preferable due to efficiency considerations. Thus, the operation on the MTPA trajectory is chosen as attraction function [27]

$$c_{A1}(k) = \left(i_d + \frac{L_d - L_q}{\psi} \left(i_d^2 - i_q^2 \right) \right)^2 \tag{7}$$

where the second term is the MTPA trajectory equation. Working on this trajectory leads to an operation with high efficiency. For operation close to the MTPA trajectory, operation off the trajectory is penalized introducing a cost, which increases with the distance to the trajectory.

Last but not least, limitations can be introduced for avoiding undesired states. The states cannot assume any value but must be limited to their rated values

$$c_{L1}(k) = \begin{cases} \left(I_r - \sqrt{i_d^2 + i_q^2} \right)^2 \left| I_r - \sqrt{i_d^2 + i_q^2} < 0 \right. \\ 0 \end{cases}. \tag{8}$$

Moreover, (7) has two solutions and it is symmetric. In order to avoid convergence to the wrong solution, the states are limited to the correct side of the symmetry axis using [27]

$$c_{L2}(k) = \begin{cases} \left(2\frac{L_d - L_q}{\psi} i_d + 1 \right)^2 \left| 2\frac{L_d - L_q}{\psi} i_d + 1 < 0 \right. \\ 0 \end{cases} \tag{9}$$

where the symmetry axis is given by the expression $2(L_d - L_q)/(\psi) i_d + 1 = 0$. The last limitation, has a minor influence on control since it avoids the case $i_d \gg 0$. Operation in this region comes along with major drawbacks: increase of flux and voltage, and reduction of the torque, i.e., it is not interesting anyway.

After the definition of the components of the cost function, the cost of each state is computed with

$$C(k) = \sum_{i=0}^{N} \begin{pmatrix} \lambda_T c_T(k+i) + \\ + \lambda_A c_A(k+i) + \\ + \lambda_L c_L(k+i) \end{pmatrix} \tag{10}$$

where λ_T, λ_A, λ_L are weighting coefficients, which defines the importance of a goal with respect to the others. The terms c_A and c_L are $c_A = c_{A1}$ and $c_L = \sum c_{Li} = c_{L1} + c_{L2}$ in the nonfield-weakening case and they are revised for operation in the field-weakening case.

B. Field Weakening Operation

For operation at high speed, the MP-DTC structure remains the same. However, the cost function must be revised. More precisely, suitable limitations and attraction regions must be introduced.

1) Limitation: The voltage must be limited according to the available voltage (5), which is given by the DC link, i.e., the rated PMSM terminal voltage $U_r = (U_c)/(\sqrt{3})$. Thus, the (speed dependent) limit is introduced

$$\xi = \sqrt{(L_q i_q)^2 + (L_d i_d + \psi)^2} - \frac{\zeta U_c}{\sqrt{3}|\omega|}$$
$$c_{L3}(k) = \begin{cases} \xi^2 | \xi < 0 \\ 0 \end{cases} \tag{11}$$

where $\zeta \in [0, 1] \subset \mathbb{R}_+$ is a safety factor.

Moreover, for avoiding stability issues at high speeds, the electrical states are limited to the space on the right of the MTPV trajectory

$$\vartheta = \frac{\psi^2}{L_q} + \psi \left(2\frac{L_d}{L_q} - 1 \right) i_d + L_d \left(\frac{L_d}{L_q} - 1 \right) i_d^2 + L_q \left(\frac{L_q}{L_d} - 1 \right) i_q^2$$
$$c_{L4}(k) = \begin{cases} \vartheta^2 | \vartheta < 0 \\ 0. \end{cases} \tag{12}$$

2) Attraction Region: Assuming the MTPA criteria as attraction region, the states will not leave the trajectory and the torque will be limited according to the voltage limit. In other words, the controller will work with reduced torque in the constant power region 1 and cannot achieve the constant power region 2 nor the reduced power region. In order to reach these regions, a path must be created close to the voltage limit in order to attract, i.e., not penalize the states for working in these conditions.

Thus, two attraction regions exists. In the constant torque region, it is the MTPA trajectory and it is an attraction to the inside of the voltage limit in the constant power region 2 and reduced power region. In the constant power region 1 both attraction regions should be active. Costs are generally summed, e.g., costs of limits c_L. However, the costs of the attraction region are generally different from zero and will influence each other. Thus, the criteria must be designed for being compatible and an exclusion function is required which decides which criteria is active.

The MTPA criteria (7) is written in the current space. For unification, the field weakening attraction region, i.e., voltage limit, is rewritten also in this space

$$c_{A2}(k) = \left(\sqrt{\left(\frac{L_q}{L_d} i_q \right)^2 + \left(i_d + \frac{\psi}{L_d} \right)^2} - \frac{\zeta U_c}{\sqrt{3}\omega L_d} \right)^2. \tag{13}$$

This unification is necessary for making the resulting costs i.e., the distances from the trajectories comparable.

At this point it is necessary to choose, which attraction region is active. The voltage limit is active, i.e., $c_A(k) = c_{A2}(k)$, if

- The state is located on the left side of the MTPA trajectory
- $c_{A2}(k) < c_{A1}(k)$

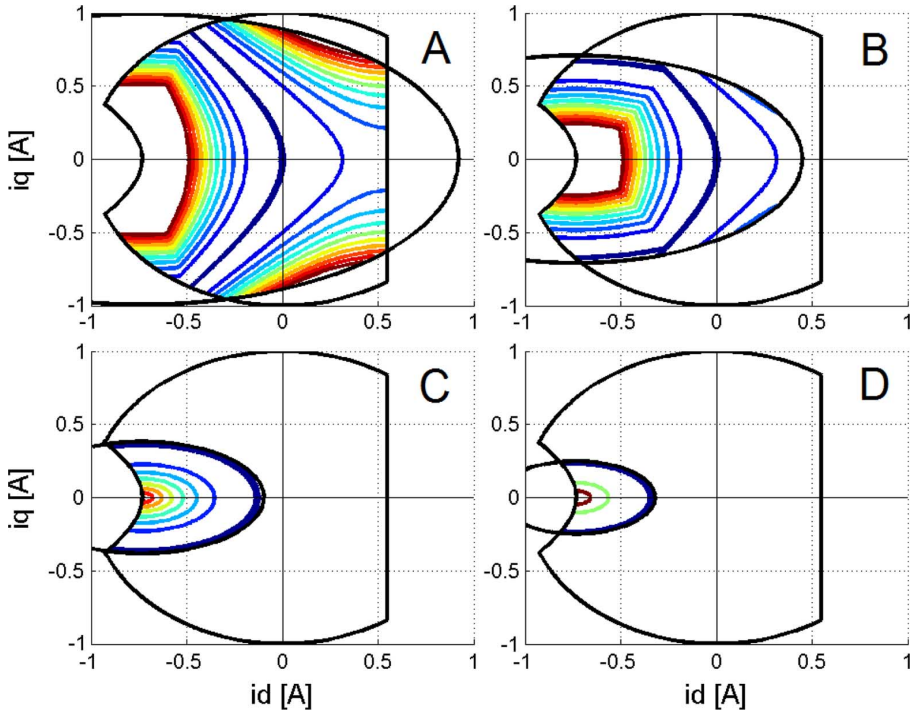

Fig. 4. Attraction region and plant limits: (A) constant torque region; (B) constant power region 1; (C) constant power region 2; (D) reduced power region.

otherwise the MTPA attraction region, i.e., $c_A(k) = c_{A1}(k)$, is active.

The costs associated to the attraction region are shown in Fig. 4, where also the limitations are shown. The regions are shown for the four cases, which depend on the speed: Fig. 4(A) constant torque region, Fig. 4(B) constant power region 1, Fig. 4(C) constant power region 2, and Fig. 4(D) reduced power region. The states are forced to stay at the inside of the region by the limitations. Preferences, where the states should stay, are expressed by the attraction region. It is given by the MTPA criteria c_{A1} in Fig. 4(A), both the MTPA c_{A1} and voltage c_{A2} criteria in Fig. 4(B), and the voltage criteria c_{A2} in Fig. 4(C) and (D).

IV. Evaluation

The concept has been developed using the simulation platform MATLAB-Simulink and it has been evaluated on an experimental test bench. The system characteristics of the PMSM-VSI drive system are shown in Table I. The DC-link has been reduced for being able to show operation in all flux weakening regions, which are:

- constant torque region: $n < 620$ rpm;
- constant power region 1 : $620 \text{ rpm} < n < 1250$ rpm;
- constant power region 2 : $1250 \text{ rpm} < n < 1400$ rpm;
- reduced power region: $n > 1400$ rpm

The experimental test bench has been designed for evaluation of power converter control systems, but it has some limitations. First, a basic 40 MHz DSP board is used for control, which has some limits in terms of calculation power. Moreover, the test bench has a diode bridge at grid side. This grid connection is suitable for operation as long energy regeneration is avoided.

TABLE I
Plant Data

Control	
Sampling time T_s	$100\mu s$
Theoretic peak switching freq. f_{swp}	$1.66kHz$
Converter	
Type	2-level VSI
DC-link voltage U_dc	$100V$
Rated current I_r	$10A$
Interlock time T_i	$1\mu s$
Electrical Machine	
Type	IPM-SM
Inductance (d axis) L_d	$12mH$
Inductance (q axis) L_q	$20mH$
Stator resistance R	$636m\Omega$
PM rotor flux ψ	$88mWb$
Pole pairs p	5
Friction constant B	$1.7 \cdot 10^{-3} kgm/s^2$
Inertia constant J	$1.0 \cdot 10^{-3} kgm^2$

A. Development

The controller has been developed in simulation assuming sufficient calculation power for $N = 5$. The performance is shown assuming a positive and negative 2000 rpm speed reference step at $t = 0.0$ s and $t = 0.6$ s, respectively. The results are shown in Fig. 5.

At low speed, the torque is constant and the acceleration is linear. At higher speed, the torque must be reduced according to the voltage limit. This happens introducing a negative d current. After reaching the reference speed n^*, the torque is reduced to a value which compensates the fiction. Moreover, the machine operates in reduced power region and the flux must be weakened also in no load conditions. Thus, a consistent current with d and q component is necessary to keep the machine in steady-state. At the inverse speed reference step the controller shows the same

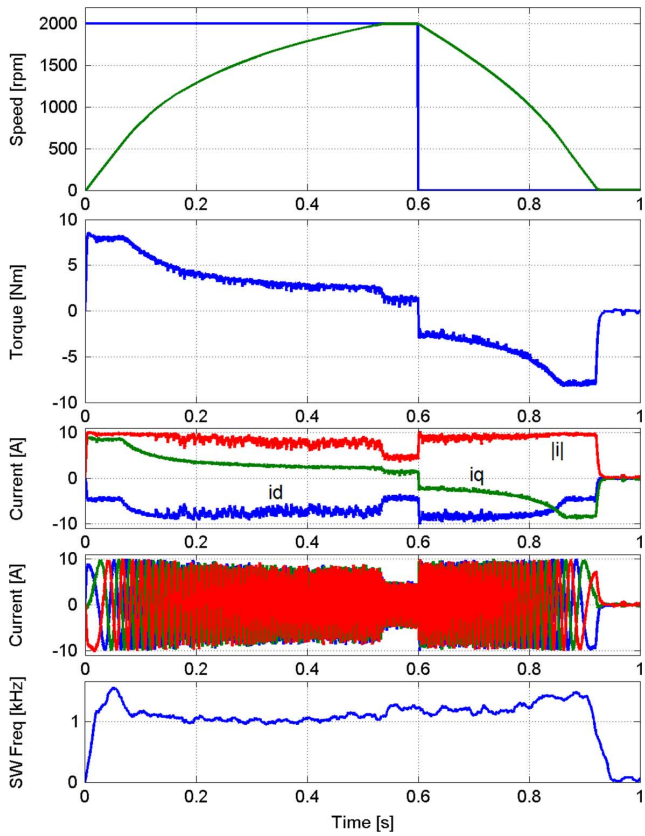

Fig. 5. Simulation result: speed reference steps with prediction horizon $N = 5$; from top: speed reference and measured speed; electromagnetic torque; absolute, d (blue), and q (green) current; phase currents; switching frequency.

behavior. Unless the fact, that at zero speed no torque for compensating the friction and no field weakening is necessary, i.e., the current is reduced to zero. Moreover, the negative reference step is faster due to friction.

The switching frequency of MP-DTC is variable. Above all medium and high power converters have a low maximum i.e., rated switching frequency due to thermal constraints. For completeness, the switching frequency is shown in Fig. 5 which stays below $f_{swp} = 1.66$ kHz.

The electrical states, which are obtained for the test in Fig. 5, are shown in Fig. 6. The states remain on the MTPA trajectory while working in the *constant torque region*. In the *constant power regions*, the states remain close to the peak current trajectory for obtaining the maximum torque with respect to a given speed. If the speed is even higher, i.e., in the *reduced power region*, the d current is not decreased anymore, and the states stay around the MTPV criteria. This operation point corresponds to the states with the peak torque, which can be obtained in this conditions. The operation in the correct region is detected and adopted automatically by the cost function.

B. Dynamic Evaluation

The prediction horizon $N = 5$ cannot be computed due to the use of the basic DSP board on the experimental test bench. Instead, the prediction horizon is reduced to $N = 1$.

The dynamic behavior has been tested applying a positive speed reference step to the system. The simulation and experimental results are shown in Fig. 7. The negative speed reference step has been avoided due to the grid connection of the converter.

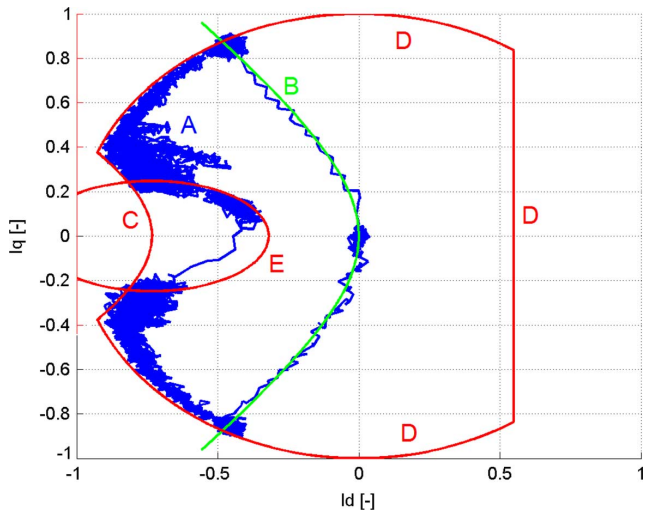

Fig. 6. Simulation result: states in the state plane of the evaluation in Fig. 5; (A) electrical states; (B) MTPA trajectory; (C) MTPV trajectory; (D) current limit; (E) voltage limit at $n = 2000$ rpm.

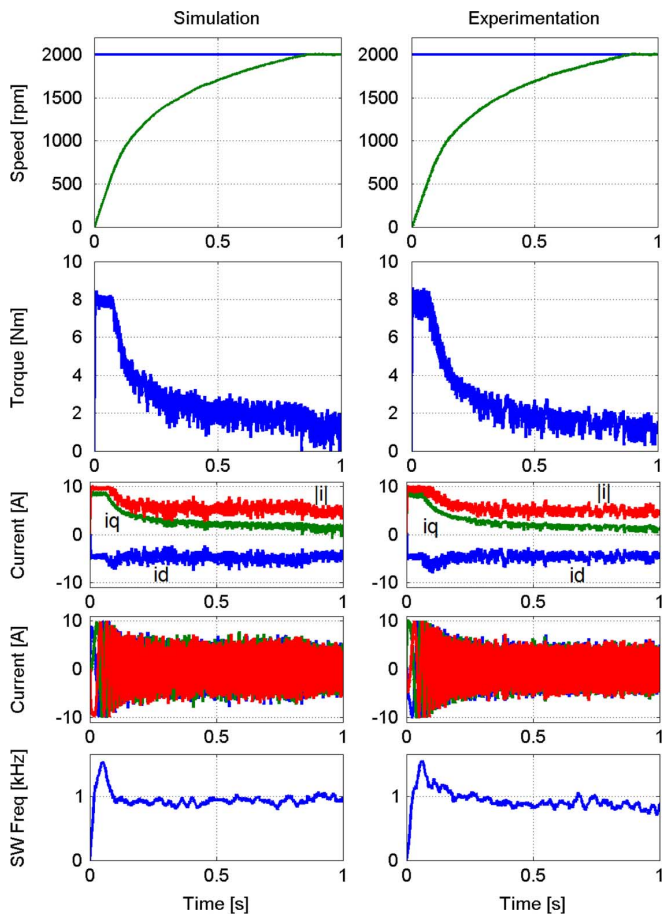

Fig. 7. Simulation and experimental result: speed reference step with prediction horizon $N = 1$; from top: speed reference and measured speed; electromagnetic torque; absolute, d (blue), and q (green) current; phase currents; switching frequency.

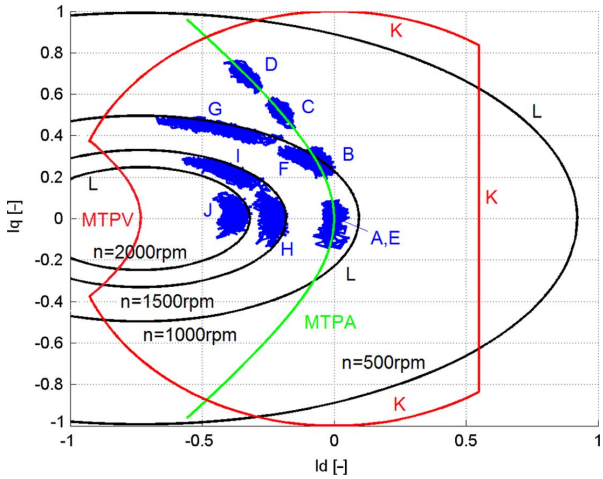

Fig. 8. Simulation result: steady-state operation points with $N = 1$: (A) $n = 500$ rpm; 0 Nm, (B) $n = 500$ rpm; 2 Nm, (C) $n = 500$ rpm, 4 Nm; (D) $n = 500$ rpm, 6 Nm; (E) $n = 1000$ rpm, 0 Nm; (F) $n = 1000$ rpm, 2 Nm; (G) $n = 1000$ rpm, 4 Nm; (H) $n = 1500$ rpm, 0 Nm; (I) $n = 1500$ rpm, 2 Nm; (J) $n = 2000$ rpm, 0 Nm; (K) current limits; (L) voltage limits.

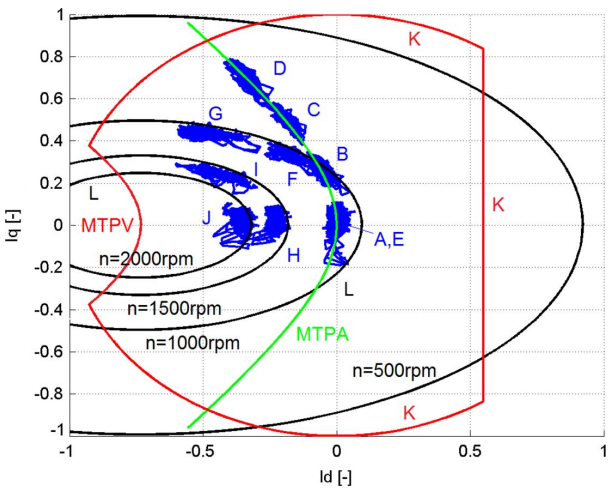

Fig. 9. Experimental result: steady-state operation points with $N = 1$: (A) $n = 500$ rpm, 0 Nm; (B) $n = 500$ rpm, 2 Nm; (C) $n = 500$ rpm, 4 Nm; (D) $n = 500$ rpm, 6 Nm; (E) $n = 1000$ rpm, 0 Nm; (F) $n = 1000$ rpm, 2 Nm; (G) $n = 1000$ rpm, 4 Nm; (H) $n = 1500$ rpm, 0 Nm; (I) $n = 1500$ rpm, 2 Nm; (J) $n = 2000$ rpm, 0 Nm; (K) current limits; (L) voltage limits.

The $N = 1$ case shows deterioration effects compared to the $N = 5$ case, i.e., the speed reference step takes more time. The reason is a less precise dynamic torque actuation at higher speeds. Moreover, a higher prediction horizon leads to a higher current, i.e., torque quality.

C. Steady-State Evaluation

Different steady-state operation points have been evaluated in order to verify the controller design. The simulation results are shown in Fig. 8 and the experimental results are shown in Fig. 9. Ideally, steady state operation with given conditions (torque, speed) would lead to a single point on the state plane. On a real system, the states stay in the neighborhood of this point due to the power converter switching.

Different load torques have been applied at different speeds:

- $n = 500$ rpm: $T_l = \{0\ \text{Nm},\ 2\ \text{Nm},\ 4\ \text{Nm},\ 6\ \text{Nm}\}$;

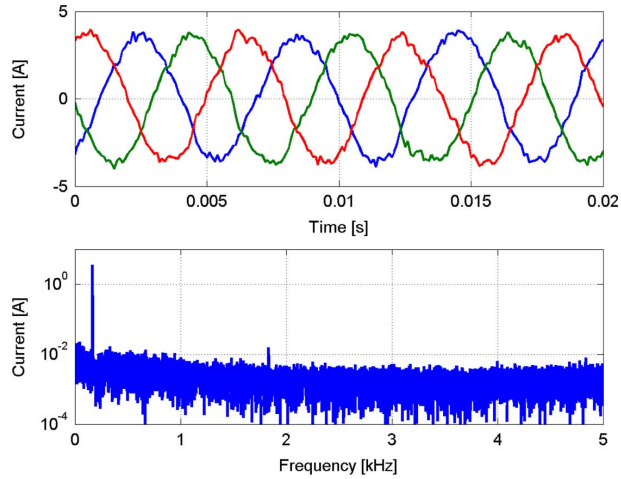

Fig. 10. Simulation result: steady-state current quality with $N = 1$, $n = 2000$ rpm, $f_{sw} = 1.3$ kHz; waveform and spectra; THD $= 2.8\%$ referred to rated current.

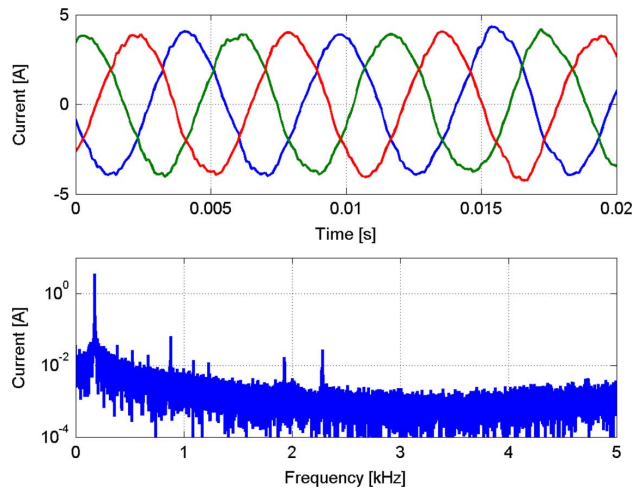

Fig. 11. Experimental result: steady-state current quality with $N = 1$, $n = 2000$ rpm, $f_{sw} = 1.3$ kHz; waveform and spectra; THD $= 2.9\%$ referred to rated current.

- $n = 1000$ rpm: $T_l = \{0\ \text{Nm},\ 2\ \text{Nm}, 4\ \text{Nm}\}$;
- $n = 1500$ rpm: $T_l = \{0\ \text{Nm},\ 2\ \text{Nm}\}$;
- $n = 2000$ rpm: $T_l = 0$ Nm

The friction has been compensated in order to gain a torque actuation which is independent from speed.

The results show an operation according to the controller synthesis. The controller operates on the MTPA trajectory in the $n = 500$ rpm case. In the $n = 1000$ rpm case, the system can operate on both, the MTPA trajectory at low torques and close to the voltage limit at higher torques. In the $n = 1500$ rpm and $n = 2000$ rpm case, the controller works also at no load in field-weakening operation.

D. Current Quality

The current quality in controllers without modulator is directly coupled with the controller design. Thus, it has been evaluated in steady-state operation. The simulation results are shown in 10 and the experimental results are shown in 11.

The spectrum has some white noise, which is given above all by the stochastic selection of the voltage vectors. Moreover,

some distinguished harmonics are found in the experimental results. They are odd harmonics and nonmultiple of three. Above all, the 5th, 11th, and 13th harmonic are pointed out.

However, amplitude of noise and harmonics are more than two decades below the amplitude of the fundamental frequency, which is more than acceptable considering $f_{sw} = 1.3$ kHz. The THD referred to the rated current is below 3%. Moreover, switching harmonics and their related noise are avoided.

On the other hand, the DC-link has been chosen low. This decision has been taken for being able to show the drive operation in the four field weakening cases without exceeding the rated speed of the PMSM. A low DC-link voltage favors generally a high current quality and deteriorations can be expected increasing U_c [23].

V. Conclusion

In this research, MP-DTC has been extended to field-weakening operation, which is required in some medium and high power drive systems, e.g., traction and power generation. MP-DTC uses the finite control set MPC approach. Plant inputs are predicted on-line and the actuation, i.e., the converter switching state, is chosen by a cost function.

The cost function has three main terms: the reference (torque) tracking, an attraction region and plant limitations. For making MP-DTC suitable for field weakening operation, the voltage limit has been added to the plant limitations. Moreover, the attraction region has been redefined. Operation on the maximum torque per ampere (MTPA) trajectory is desirable at low speed. At high speeds, operation off the MTPA trajectory is necessary for obtaining field weakening. However, operation with the lowest admissible current is still aimed.

MP-DTC in field-weakening operation has been evaluated in simulation and experimentally. The dynamic performance has been evaluated applying a speed reference step to the system. Moreover, steady-state operation is shown in the cases: *constant torque operation*, *constant power operation* and *reduced power operation* applying different load torques. The controller shows generally satisfactory results and a good correspondence between design, simulation, and experimentation.

Separately, the steady-state current quality has been evaluated. Harmonics and noise are about two decades below the amplitude of the fundamental frequency. Thus, the current quality is satisfactory for most applications, above all considering the the switching frequency, which will not exceed 1.66 kHz (theoretical maximum value), i.e., 1.3 kHz (steady-state average value in the case $n = 2000$ rpm).

The MP-DTC performance in field weakening operation can be further improved using more powerful controller hardware. In further work, a substitution of the actual control hardware is planned.

Appendix
MTPV Criteria

The *Maximum Torque per Volt* criteria gives the peak torque, which can be obtained at a given voltage. Assuming steady state conditions and infinitesimal resistances the PMSM terminal voltage is

$$u^2 = (\omega L_q i_q)^2 + (\omega L_d i_d + \psi)^2 \tag{14}$$

which is an ellipsis, with the center in $[i_d, i_q] = [0, -(\psi)/(L_d)]$. The coordinate transformation

$$\begin{aligned} i_d &= i'_d - \frac{\psi}{L_d} \\ i_q &= i'_q \frac{L_d}{L_q} \end{aligned} \tag{15}$$

transforms the ellipsis in a circle with center in the origin, i.e.,

$$u^2 = (\omega L_d i'_q)^2 + (\omega L_d i'_d)^2. \tag{16}$$

The torque equation in the $d'q'$ coordinate system is

$$T = \frac{3}{2} p(\psi i'_q + (L'_d - L'_q) i'_d i'_q) \tag{17}$$

where $L'_d = (L_d^2)/(L_q)$ and $L'_q = L_d$. Transforming into polar coordinates

$$\begin{aligned} i'_d &= I' \sin(\delta') \\ i'_q &= I' \cos(\delta') \end{aligned} \tag{18}$$

the MTPV condition can be obtained by its definition

$$\frac{\partial T}{\partial \delta'} = 0. \tag{19}$$

The solution is already known from the MTPA criteria (in the dq-system), which is

$$\psi i'_d + \left(L'_d - L'_q\right)\left(i'^2_d - i'^2_q\right) = 0. \tag{20}$$

Transforming into the dq-system, the MTPV condition becomes

$$\begin{aligned} \frac{\psi^2}{L_q} + \psi \left(2\frac{L_d}{L_q} - 1\right) i_d \\ + L_d \left(\frac{L_d}{L_q} - 1\right) i_d^2 + L_q \left(\frac{L_q}{L_d} - 1\right) i_q^2 = 0. \end{aligned} \tag{21}$$

References

[1] J. Maciejowski, *Predictive Control With Constraints*. Englewood Cliffs, NJ: Prentice Hall, 2002.

[2] A. Linder, R. Kanchan, R. Kennel, and P. Stolze, *Model-Based Predictive Control of Electric Drives*. Berlin, Germany: Cuvillier Verlag Gttingen, 2010.

[3] S. Bolognani, S. Bolognani, L. Peretti, and M. Zigliotto, "Design and implementation of model predictive control for electrical motor drives," *IEEE Trans. Ind. Electron.*, vol. 56, no. 6, pp. 1925–1936, Jun. 2009.

[4] T. Geyer, "Computationally efficient model predictive direct torque control," *IEEE Trans. Power Electron.*, vol. 26, no. 10, pp. 2804–2816, Oct. 2011.

[5] M. Preindl, E. Schaltz, and P. Thgersen, "Switching frequency reduction using model predictive direct current control for high power vsi," *IEEE Trans. Ind. Electron.*, vol. 58, no. 7, pp. 2826–2835, Jul. 2010.

[6] R. Errouissi, M. Ouhrouche, W. Chen, and A. Trzynadlowski, "Robust nonlinear predictive controller for permanent magnet synchronous motors with optimized cost function," *IEEE Trans. Ind. Electron.*, vol. 58, no. 7, pp. 1–1, Jul. 2011.

[7] S. Mariethoz, A. Domahidi, and M. Morari, "Sensorless explicit model predictive control of permanent magnet synchronous motors," in *Proc. IEEE IEMDC*, May 2009, pp. 1250–1257.

[8] T. Geyer, "A comparison of control and modulation schemes for medium-voltage drives: Emerging predictive control concepts versus pwm-based schemes," *IEEE Trans. Ind. Appl.*, vol. 47, no. 3, pp. 1380–1389, Mar. 2011.
[9] M. Kazmierkowski and L. Malesani, "Current control techniques for three-phase voltage-source pwm converters: A survey," *IEEE Trans. Ind. Electron.*, vol. 45, no. 5, pp. 691–703, Oct. 1998.
[10] T. Geyer, G. Papafotiou, and M. Morari, "Model predictive direct torque control—Part 1: Concept, algorithm, and analysis," *IEEE Trans. Ind. Electron.*, vol. 56, no. 6, pp. 1894–1905, Jun. 2009.
[11] G. Papafotiou, J. Kley, K. Papadopoulos, P. Bohren, and M. Morari, "Model predictive direct torque control—Part 2: Implementation and experimental evaluation," *IEEE Trans. Ind. Electron.*, vol. 56, no. 6, pp. 1894–1905, Jun. 2009.
[12] P. Corts, M. P. Kazmierkowski, R. M. Kennel, D. E. Quevedo, and J. Rodrguez, "Predictive control in power electronics and drives," *IEEE Trans. Ind. Electron.*, vol. 55, no. 12, pp. 4312–4324, Dec. 2008.
[13] J.-O. Krah and J. Holtz, "High-performance current regulation and efficient pwm implementation for low-inductance servo motors," *IEEE Trans. Ind. Appl.*, vol. 35, no. 5, pp. 1039–1049, Sep.–Oct. 1999.
[14] H. Liu and S. Li, "Speed control for pmsm servo system using predictive functional control and extended state observer," *IEEE Trans. Ind. Electron.*, vol. 58, no. 2, pp. 1171–1183, Feb. 2011.
[15] S. Mariethoz and M. Morari, "Explicit model-predictive control of a pwm inverter with an lcl filter," *IEEE Trans. Ind. Electron.*, vol. 56, no. 2, pp. 389–399, Feb. 2009.
[16] M. Perez, J. Rodriguez, E. Fuentes, and F. Kammerer, "Predictive control of ac-ac modular multilevel converters," *IEEE Trans. Ind. Electron.*, vol. 58, no. 7, pp. 2832–2839, Jul. 2011.
[17] M. Pacas and J. Weber, "Predictive direct torque control for the pm-synchronous machine," *IEEE Trans. Ind. Electron.*, vol. 52, no. 5, pp. 1350–1356, Oct. 2005.
[18] J. Beerten, J. Verveckken, and J. Driesen, "Predictive direct torque control for flux and torque ripple reduction," *IEEE Trans. Ind. Appl.*, vol. 57, no. 1, pp. 404–412, Jan. 2010.
[19] J. Holtz and S. Stadtfeld, "A predictive controller for the stator current vector of ac machines fed from a switched voltage source," in *Proc. IPEC*, 1983, pp. 1665–1675.
[20] I. Takahashi and T. Noguchi, "A new quick response and high efficiency control strategy of an IM," in *Proc. IEEE IAS*, 1985, pp. 1665–1675.
[21] M. Barcaro, E. Fornasiero, N. Bianchi, and S. Bolognani, "Design procedure of ipm motor drive for railway traction," in *Proc. IEEE Int. Electr. Mac., Drives Conf. (IEMDC)*, 2011, pp. 983–988.
[22] N. Bianchi, S. Bolognani, and B. Ruzojcic, "Design of a 1000 hp permanent magnet synchronous motor for ship propulsion," in *Proc. 13th Eur. Conf. Power Electron. Appl. (EPE'09)*, 2009, pp. 1–8.
[23] M. Preindl and S. Bolognani, "Optimized design of two and three level full-scale voltage source converters for multi-mw wind power plants at different voltage levels," in *Proc. IECON 2011—37th Annu. Conf. IEEE Ind. Electron. Soc.*, 2011, pp. 3634–3639.
[24] S. Bolognani, S. Calligaro, R. Petrella, and F. Pogni, "Flux-weakening in ipm motor drives: Comparison of state-of-art algorithms and a novel proposal for controller design," in *Proc. 2011-14th Eur. Conf. Power Electron. Appl. (EPE 2011)*, 2011, pp. 1–11.
[25] M. Zordan, P. Vas, M. Rashed, S. Bolognani, and M. Zigliotto, "Field-weakening in high-performance pmsm drives: A comparative analysis," in *Proc. IEEE Conf Ind. Appl. Conf. Record*, 2000, vol. 3, pp. 1718–1724.
[26] R. P. Aguilera and D. E. Quevedo, "On stability and performance of finite control set mpc for power converters," in *Proc. Workshop Predictive Contr. Electri. Drives Power Electron. (PRECEDE)*, 2011.
[27] "Model predictive direct torque control with finite control set for pmsm drive systems, Part 1: maximum torque per ampere operation," *IEEE Trans. Ind. Inf.*, 2012, to be published.
[28] P. Cortes, J. Rodriguez, C. Silva, and A. Flores, "Delay compensation in model predictive current control of a three-phase inverter," *IEEE Trans. Ind. Electron.*, vol. 59, no. 2, pp. 1323–1325, Feb. 2011.
[29] R. Kalman, "A new approach to linear filtering and prediction problems," *J. Basic Eng.*, vol. 82, pp. 35–45, 1960.
[30] D. Luenberger, "Observing the state of a linear system," *IEEE Trans. Mil. Electron.*, vol. 8, pp. 74–80, 1964.

Matthias Preindl was born in Brixen, Italy, in 1986. He received the B.Sc. degree (*summa cum laude*) from the University of Padova, Padova, Italy, in 2008, and the M.Sc. degree from ETH Zurich, Zurich, Switzerland, in 2010, both in electrical engineering. He has been visiting student at Aalborg University, Denmark where he wrote his diploma thesis. He is currently working towards the Ph.D. degree in energy engineering at University of Padova.

He is currently a Visiting Scholar at University of California, Berkeley. From 2010 to 2012, he was with Leitwind AG, Italy, where he was an R&D Engineer. Before that, he worked for Energy.dis GmbH, Italy and the Italian National Research Council (CNR-RFX). His research interests include control and design of power electronic systems with applications in drive systems, renewable energy generation, and vehicular systems.

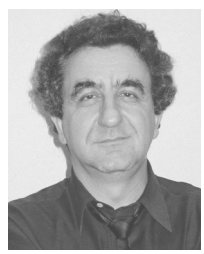

Silverio Bolognani (M'76) received the Laurea degree in electrical engineering from the University of Padova, Padova, Italy, in 1976.

In 1976, he joined the Department of Electrical Engineering at the University of Padova, where he is currently a Full Professor of Electrical Converters, Machines, and Drives. He then started the Electrical Drives Laboratory, where a variety of research works on brushless and induction motor drives is carried out in the frame of the European and the national research projects. He is the author of more than 200 papers on electrical machines and drives and is the holder of three patents. He is currently the Chairman of the IEEE North Italy IEEE Industry Applications/Industrial Electronics/Power Electronics Societies Joint Chapter. He has been serving international conferences as a Member of the Steering or Technical Committees, as well as an Invited Speaker.